Analysis of converted-wave extended images for migration velocity analysis

Jia Yan & Paul Sava, Center for Wave Phenomena, Colorado School of Mines

SUMMARY

Converted-wave data have been recognized to have potential in complementing conventional compressional data. However, imaging for converted-waves is more difficult mainly due to the need for estimating shear-wave velocities, in addition to compressional-wave velocities. The common practice is to obtain the shear-wave velocity by registering PS and PP images. Despite its low cost, this procedure is prone to error due to the assumption of imaging simple structure and due to the high potential for cycle skipping. On the other hand, we could obtain S velocities by adapting wave-equation migration velocity analysis (MVA) tools for shear waves. We derive the moveout function for CIPs of converted-wave images and find that they present more complicated moveout than their pure-mode counterparts. We explore the applicability of differential semblance optimization (DSO) to the PP and PS CIP gathers to obtain objective functions, based on which we can construct optimal velocity models. We find that the objective functions for both PP and PS data are convex, which warrants their use for migration velocity analysis using efficient gradient-descent numerical optimization schemes.

INTRODUCTION

Multicomponent data are acquired both on land and at ocean bottom because converted-waves have been recognized to have potential advantages in several aspects. Converted waves can produce better images of the Earth structure where P-waves have small reflectivity and S-waves have larger reflectivity. Converted waves also complement P-waves in imaging through zones where P-waves are highly attenuated and S-waves are less affected, e.g., gas-concentrated area. Converted-waves also provide invaluable information for lithology estimations, anisotropy parameter estimations, and reservoir characterization (Stewart et al., 2002, 2003).

Many authors, including Nicoletis et al. (1998), Kendall et al. (1998), and Dai et al. (2000), investigate methods for time or depth migration using converted-wave data. The migration procedures for PP and PS data do not differ in nature, and both include two basic steps: the reconstruction of source and receiver wavefields at all locations in the subsurface and the application of an imaging condition to extract reflectivity from the reconstructed wavefields. The main difference is that for PP data, both source and receiver wavefields are reconstructed using P-wave velocity; for PS data, source and receiver wavefields are reconstructed with P- and S-wave velocities, respectively.

The velocity estimation for shear-waves is mostly carried out by the so-called "registration" process: shear-wave velocities are estimated or tuned by correlating corresponding PP and PS reflections in the time-migrated seismic sections and stretching in time the PS section to match with the PP section using the estimated V_P/V_S ratio (Gaiser, 1996; Ogiesoba and Stewart, 2003; Fomel and Backus, 2003; Nickel and Sonneland, 2004; Fomel et al., 2005; Yuan et al., 2008). The registration technique has the benefit of fast performance because the operation is usually carried out in the time domain and is relatively not time-consuming. However, velocity analysis using image registration has some inherent problems, such as that P- and S-waves are assumed to have similar reflectivity in a long-wavelength scale, and that the process is prone to cycle-skipping without the aid of well logs.

We explore the possibility of wave-equation MVA in the depth domain for the shear-mode using converted-wave data only, i.e., we update the S velocity after P velocity analysis, while keeping the P velocity fixed. We assume that the velocity of the P-wave is known from MVA of the PP component of the data, and then we perform MVA on the PS component only.

Wave equation migration velocity analysis (WEMVA) exploits the errors from extended images due to the incorrect migration velocity. Subsets of extended images can be organized as common-image gathers (CIGs) (Rickett and Sava, 2001; Yang and Sava, 2008; Sava and Fomel, 2003; Yan and Sava, 2008) or common-image point gathers (CIPs) (Sava and Vasconcelos, 2010). Sava and Vasconcelos (2010) develop the concept of CIPs and argue that computational cost for constructing CIPs decreases compared to the cost of constructing regular CIGs. They derive the moveout function of CIP events for pure-mode and suggest their use for migration velocity analysis (MVA). In this paper, we derive the moveout of CIPs for converted-waves, discuss their features, and compare the CIPs for pure-mode and converted-mode waves. We find that compared to PP CIPs, the PS CIPs are characterized by more complicated moveout, which increases the difficulty of using them for migration velocity analysis. We formulate DSO type penalty functions (Shen and Symes, 2008) for pure- and converted-mode data and show that the corresponding objective functions are convex functions suitable for numerical optimization with gradient based techniques.

COMMON IMAGE POINT GATHERS

In this section, we derive the moveout equation for common image point (CIP) gathers for converted-waves, assuming imaging with both a single shot and multiple shots. The moveout functions offer insight into the expected behavior of such CIPs in areas of complex velocity variations (Sava and Vasconcelos, 2010) and form the basis for the definition of an objective function for migration velocity analysis.

CIP moveout for imaging with a single shot

We use Figure 1 to illustrate the notations adopted in our derivation. In this cartoon, the vector $\mathbf{q}$ denotes the direction along which the reflector and the reflection plane intersect, and the

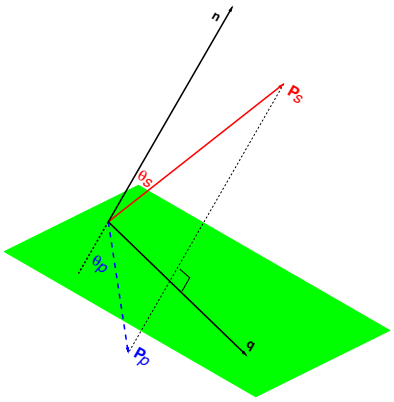

Figure 1: A cartoon illustrating a P to S reflection upon a reflector. The reflection plane and the reflector intersect along a line defined by the vector $\mathbf{q}$. The reflector has a normal defined by the vector $\mathbf{n}$. The source and receiver rays are characterized by the vectors $\mathbf{p}_p$ and $\mathbf{p}_s$, respectively. The incidence and reflection angles are denoted by θ_p and θ_s, respectively.

vector $\mathbf{n}$ denotes the reflector normal. For a P-wave ray vector $\mathbf{p}_p$ incident upon the reflector at an angle θ_p, the S-wave ray $\mathbf{p}_s$ is reflected at an angle θ_s. The incidence and reflection angles are related by the Snell's law:

$$\frac{\sin\theta_p}{v_p} = \frac{\sin\theta_s}{v_s}\,, \tag{1}$$

where v_p and v_s are the P- and S-wave velocities, respectively. The Snell's law simply states that the slowness along the reflector is preserved regardless of the reflector dip. We can express the source and receiver ray vectors as $\mathbf{p}_p = \frac{\mathbf{n}_p}{v_p}$ and $\mathbf{p}_s = \frac{\mathbf{n}_s}{v_s}$, where $\mathbf{n}_p$ and $\mathbf{n}_s$ are unit vectors along the source and receiver rays, respectively.

We begin with the conventional imaging condition for P to S reflection. For a subsurface image point $\mathbf{x}$, the conventional imaging condition can be expressed as the intersection of two planes given by the expressions

$$\mathbf{p}_p \cdot \mathbf{x} = 0\,, \tag{2}$$
$$\mathbf{p}_s \cdot \mathbf{x} = 0\,. \tag{3}$$

These relations assume that we take the origin of the space-time coordinate system at the image point $\mathbf{x}$. The extended imaging condition shifts the source and receiver planes in space by the space-lag $\boldsymbol{\lambda}$ in the positive and negative directions, respectively, and in time by τ_p and τ_s, respectively:

$$\mathbf{p}_p \cdot (\mathbf{x} - \boldsymbol{\lambda}) = -\tau_p\,, \tag{4}$$
$$\mathbf{p}_s \cdot (\mathbf{x} + \boldsymbol{\lambda}) = +\tau_s\,. \tag{5}$$

Since the source and receiver wavefields have a time separation 2τ, we have $\tau_p + \tau_s = 2\tau$. Combining the expressions 2 to 5, we obtain:

$$(\mathbf{p}_p + \mathbf{p}_s) \cdot \boldsymbol{\lambda} = 2\tau\,. \tag{6}$$

We can also express the vectors $\mathbf{p}_p$ and $\mathbf{p}_s$ using the geometric relations between the vectors $\mathbf{n}$ and $\mathbf{q}$ and angles θ_p and θ_s as:

$$\mathbf{p}_p = \frac{\sin\theta_p}{v_p}\mathbf{q} - \frac{\cos\theta_p}{v_p}\mathbf{n}\,, \tag{7}$$
$$\mathbf{p}_s = \frac{\sin\theta_s}{v_s}\mathbf{q} + \frac{\cos\theta_s}{v_s}\mathbf{n}\,. \tag{8}$$

Substitution of equations 7 and 8, together with the Snell's law from equation 1, into equation 6 yields the expression

$$\sin\theta\,(\mathbf{q}\cdot\boldsymbol{\lambda}) + \frac{1}{2}\left[\sqrt{\gamma^2 - \sin^2\theta} - \cos\theta\right](\mathbf{n}\cdot\boldsymbol{\lambda}) = v\tau\,, \tag{9}$$

where the angle θ denotes the incidence angle θ_p, the variable v is the P-wave velocity v_p, and the variable γ is the ratio between the P- and S-wave velocities. For the special case of PP reflections, where $\gamma = 1$, equation 9 reduces to

$$\sin\theta\,(\mathbf{q}\cdot\boldsymbol{\lambda}) = v\tau\,, \tag{10}$$

which is the relation described by Sava and Vasconcelos (2010). Equation 9 describes the moveout function characterizing a reflection from a single shot-receiver pair. The function represents a plane in the $\{\boldsymbol{\lambda}, \tau\}$ space which depends on the incidence angle, the P-wave velocity, the v_p/v_s ratio, and the reflector defined by the vectors $\mathbf{q}$ and $\mathbf{n}$.

To confirm the validity of equation 9, we overlay this function on a CIP reflection shown in Figure 2 for a horizontal reflector (Figure 2(a)). In Figures 2(a), the dot on the surface at $x = 3.1$ km represent the source and the line on the surface represent the receivers. The dot on the reflector indicate the CIP location. Panel (b) and shows the PP and PS reflections as a function of $\boldsymbol{\lambda}$ and τ. The lines overlaid on top of these subplots indicate that equation 9 accurately predicts the CIP moveout.

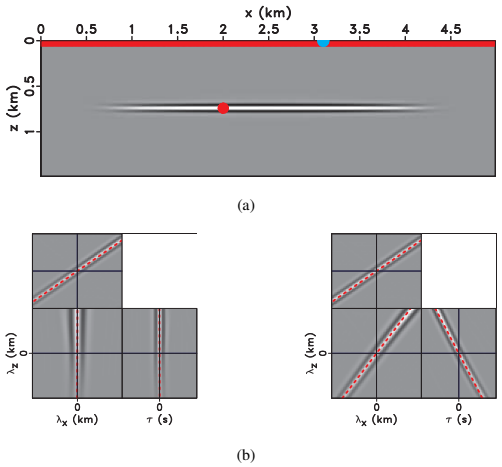

Figure 2: (a)The experiment geometry used to construct the CIP gathers in panel (b). The dot on the surface represents the shot location, the line on the surface represents the receivers, and the dot on the reflector represents the CIP location. A common image point reflection for PP (left) and PS (right) data for the experiment shown in Figure 2(a). The overlain dashed line is given by equation 9 and matches exactly with the CIP reflection moveout.

CIP moveout for imaging with multiple shots

The CIP moveout for multiple shots can be analyzed as the superposition of single-shot CIPs constructed for different angles of incidence. In the following, we consider the reflection geometries in the reflection plane, thus setting the y component of all vectors to zero. Since the vector $\mathbf{q}$ and the reflector normal vector $\mathbf{n}$ are orthogonal, we can write $\mathbf{q} = \{q_x, q_z\}$ and $\mathbf{n} = \{-q_z, q_x\}$. With the substitution of the $\mathbf{q}$ and $\mathbf{n}$ components into equation 9, we can write

$$(Aq_x - Bq_z)\,\lambda_x + (Aq_z + Bq_x)\,\lambda_z - \lambda_\tau = 0\,, \qquad (11)$$

where $A = \sin\theta$, $B = \frac{1}{2}\left[\sqrt{\gamma^2 - \sin^2\theta} - \cos\theta\right]$, and $\lambda_\tau = v\tau$. Equation 11 states that the CIP moveout for a single shot is represented by a plane that passes through the origin of the lag space $\{\boldsymbol{\lambda}, \lambda_\tau\}$ and is characterized by the vector normal. When we consider multiple shots, the CIP moveout can be measured on the superposition of all single-shot CIP reflection planes for various angles of incidence θ. Let us consider reflections from two nearby shots whose vector normals are $\mathbf{v}_1$ and $\mathbf{v}_2$, respectively. When the incidence angle changes from θ to $\theta + d\theta$, the two CIP reflection planes from neighboring shots intersect along a line. The cross product of the two vector normals $\mathbf{v}_1$ and $\mathbf{v}_2$ gives a vector $\mathbf{V}$, which is parallel to the intersection line. Since both planes pass through the origin, the intersection line also passes through the origin. Thus, we can simply use the vector $\mathbf{V}$ originating at the origin to represent the intersection line of two neighboring CIP reflection planes. The moveout surface for a CIP gather is the ensemble of the intersection lines for all possible incidence angles.

To derive the intersection line formula for two adjacent CIP reflection planes, we begin by explicitly writing the vector normals of the planes from two neighboring shots:

$$\mathbf{v}_i = \left(A_i q_x - B_i q_z, A_i q_z + B_i q_x, -1\right)\,, \qquad (12)$$

where the subscript $i = 1, 2$ for two incidences, and the incidence angle θ for the two incidences are θ and $\theta + d\theta$, respectively.

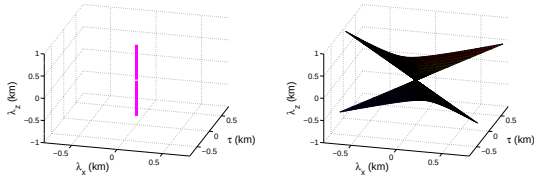

Figure 3: Panels (c) and (d) represent the CIP line and surface predicted by the moveout equations 14 and 13, respectively.

By neglecting the quadratic terms $(d\theta)^2$ in the cross product of $\mathbf{v}_1$ and $\mathbf{v}_2$, and by scaling the cross product by an arbitrary quantity r, we obtain the parametric form of the PS CIP surface

$$CIP_{PS}(r,\theta,\alpha,\gamma) = r \begin{pmatrix} \frac{1}{2}\tan\theta\left(1 - \frac{\cos\theta}{\sqrt{\gamma^2 - \sin^2\theta}}\right)\cos\alpha + \sin\alpha \\ \frac{1}{2}\tan\theta\left(1 - \frac{\cos\theta}{\sqrt{\gamma^2 - \sin^2\theta}}\right)\sin\alpha - \cos\alpha \\ \frac{1}{2\cos\theta}\left(1 - \frac{\gamma^2\cos\theta}{\sqrt{\gamma^2 - \sin^2\theta}}\right) \end{pmatrix}^{\mathrm{T}} \qquad (13)$$

where r can take positive and negative values. The surface reduces to the simple form

$$CIP_{PP}(r,\theta,\alpha,\gamma = 1) = r\left(\sin\alpha, -\cos\alpha, 0\right) \qquad (14)$$

for pure wave-modes.

Figure 3 shows PP and PS reflections CIPs for a horizontal reflector. Figures 3(a) and (b) represent the CIP line and surface for PP and PS reflections given by equations 14 and 13, respectively. The PS CIP is a smooth surface symmetric about the $\lambda_x = 0$ plane and reduces to a line along the λ_z axis for pure-mode reflections.

OBJECTIVE FUNCTION FOR CIPS

In order to obtain an optimized migration velocity model, an objective function that reaches its minimum at correct velocity is needed. Shen et al. (2003), Shen (2004), and Shen and Symes (2008) propose the use of differential semblance criteria to formulate the objective function. A differential semblance optimization (DSO) operator P defines a residual by penalizing the departure of image gathers from an ideal shape corresponding to the image constructed with correct velocity. The application of an operator P to the extended images $R(\mathbf{x}, \boldsymbol{\lambda}, \tau)$ at incorrect velocity gives an image residual. Thus, the optimization problem can be formulated by minimizing the objective function:

$$J = \frac{1}{2}\|P[R]\|\,. \qquad (15)$$

In particular, the objective function for wave-equation migration velocity analysis can be constructed for subsets of extended images CIGs or CIPs. We show the formulation of an objective function for CIP gathers.

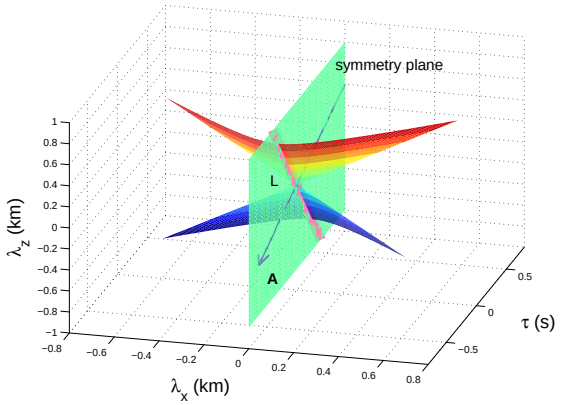

Figure 4: A cartoon showing the quantities used to define a penalty function for PS CIPs. For simplicity, we use a horizontal reflector in this cartoon. The curved surface is the CIP surface for PS data, and the plane $\lambda_x = 0$ is the symmetry axis of the surface. The CIP surface and its symmetry axis intersect along the line L. In the symmetry plane, we can find a vector $\mathbf{A}$ perpendicular to the line L.

The simple form of the CIP for PP extended images (equation 14) allows for an easy formulation of a penalty function.

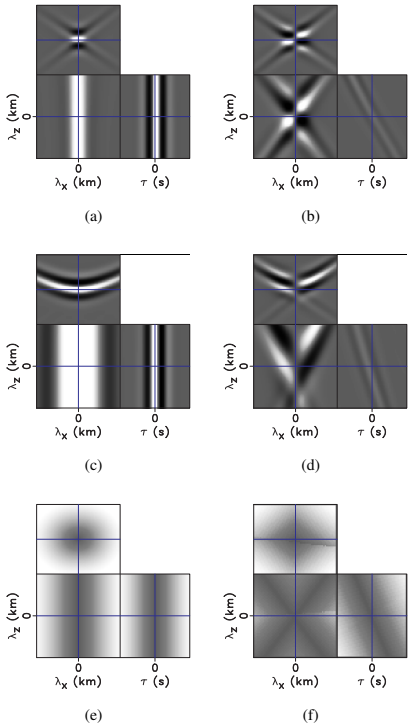

Figure 5: Panels (a) and (b) show CIG gathers for PP and PS data, respectively, obtained with correct velocity. Panels (c) and (d) are the PP and PS CIG gathers for incorrect velocities. The (e) PP and (f) PS penalty functions are given by equations 16 and 19, respectively.

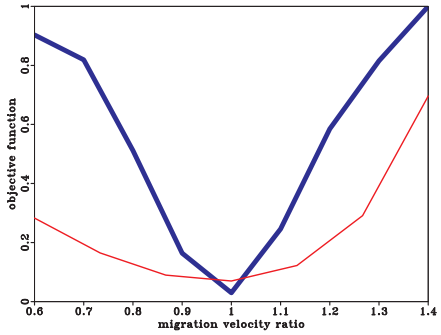

Figure 6: Objective function for PP and PS CIPs by applying the penalty functions, Figure 5(e) and (f), to PP and PS CIP gathers respectively. The thick line is for PP data, and the thin line is for PS data. The horizontal axis is the ratio of migration velocity and true model velocity. The PS CIP gathers are obtained using correct P-wave velocity.

A possible penalty function can be written as

$$P_{(\boldsymbol{\lambda},\lambda_\tau)}[R] = R\sqrt{(\mathbf{q}\cdot\boldsymbol{\lambda})^2 + \lambda_\tau^2}\,, \qquad (16)$$

which penalizes by the radial distance from the PP CIP line.

Similarly, for PS gathers we can define a penalty function which increases with distance from the surface defined by equation 13. From equation 13, the symmetry plane of the PS CIP surface intersects the surface at the incidence angle $\theta = 0$. The intersection line is given by

$$L(\gamma,\alpha) = r\left(-\sin\alpha, -\cos\alpha, \tfrac{1-\gamma}{2}\right)\,, \qquad (17)$$

A vector perpendicular to this intersection line in the symmetry plane is:

$$\mathbf{A}(\gamma,\alpha) = \left(\tfrac{\gamma-1}{2}\sin\alpha, \tfrac{\gamma-1}{2}\cos\alpha, -1\right)\,. \qquad (18)$$

The vector $\mathbf{A}$ is an axis used for measuring the distance from the CIP surface. Based on the geometry shown in Figure 4, we construct a penalty function as the superposition of shifted CIP surfaces corresponding to various distances from the surface defined by equation 13. These surfaces in the $\{\boldsymbol{\lambda},\tau\}$ space are both shifted by a distance d along the axis vector $\mathbf{A}(\gamma,\alpha)$ and also scaled by a factor $|d|$. A possible CIP penalty function is thus given by the parametric form

$$\begin{aligned} & P_{(\lambda_x,\lambda_z,\lambda_\tau,\alpha,\gamma)}[R] \\ = \;& P_{(\lambda_x(r,\theta),\lambda_z(r,\theta),\lambda_\tau(r,\theta),\alpha,\gamma)}[R] \\ = \;& R\sum_d |d|\cdot\left[CIP_{PS}(r,\theta,\alpha,\gamma) - d\frac{\mathbf{A}(\gamma,\alpha)}{|\mathbf{A}(\gamma,\alpha)|}\right] \end{aligned} \qquad (19)$$

Here, d ranges from negative to positive values along the axis defined by vector $\mathbf{A}(\gamma,\alpha)$.

We plot the PP (equation 16) and PS (equation 19) penalty functions in Figure 5 for a horizontal reflector. The penalty function is zero at the CIP line/surface (shown in Figures 5(a) and (b) for horizontal reflector). Figure 6 shows the objective function $J = \frac{1}{2}\|P_{(\boldsymbol{\lambda},\lambda_\tau)}[R]\|$ for both PP and PS data. The well behaved convex functions indicate that the formulated penalty functions can be used for migration velocity analysis.

CONCLUSIONS

We study the features of common image point gathers for converted-waves. For correct migration velocities, the CIPs for pure wave-modes are characterized by a line in the space- and time-lag space oriented orthogonal to the reflector; the CIPs for converted-waves are characterized by surfaces which contain the origin of the space- and time-lag space. For incorrect migration velocities, the PP CIPs are not characterized by focused lines but by surfaces which depend on the migration velocities; the PS CIPs are also characterized by surfaces deviating from their ideal shape corresponding to correct velocity. The deviation of CIPs gathers obtained with incorrect migration velocities from the ones obtained with correct migration velocities warrants their use for migration velocity analysis. We use differential semblance optimization (DSO) to define penalty functions for PP and PS CIPs. We formulate objective functions by penalizing the departure of the gathers from the ideal shape obtained with correct migration velocities. The objective functions for both PP and PS data are convex, which allows their use in velocity optimization using gradient-descent methods.

ACKNOWLEDGMENTS

We acknowledge the financial support of the sponsors of the Center for Wave Phenomena at Colorado School of Mines. The reproducible numeric examples in this paper use the Madagascar open-source software package freely available from `http://www.reproducibility.org`.

REFERENCES

Dai, H., X. Y. Li, and M. Mueller, 2000, Compensating for the effects of gas clouds by prestack migration: A case study from Valhall: 70th Ann. Internat. Mtg, Soc. of Expl. Geophys., 1047–1050.

Fomel, S., M. Backus, K. Fouad, B. Hardage, and G. Winters, 2005, A multistep approach to multicomponent seismic image registration with application to a West Texas carbonate reservoir study: SEG Technical Program Expanded Abstracts, **24**, 1018–1021.

Fomel, S., and M. M. Backus, 2003, Multicomponent seismic data registration by least squares: SEG Technical Program Expanded Abstracts, **22**, 781–784.

Gaiser, J. E., 1996, Multicomponent Vp/Vs correlation analysis: Geophysics, **61**, 1137–1149.

Kendall, R. R., S. H. Gray, and G. E. Murphy, 1998, Subsalt imaging using prestack depth migration of converted waves: Mahogany Field, Gulf of Mexico: 68th Ann. Internat. Mtg, Soc. of Expl. Geophys., 2052–2055.

Nickel, M., and L. Sonneland, 2004, Automated PS to PP event registration and estimation of a high-resolution Vp-Vs ratio volume: 74th Ann. Internat. Mtg., Soc. of Expl. Geophys., 869–872.

Nicoletis, L. M., J. Svay-Lucas, and H. Prigent, 1998, True amplitude pre-stack imaging of converted waves: 68th Ann. Internat. Mtg, Soc. of Expl. Geophys., 734–737.

Ogiesoba, O. C., and R. R. Stewart, 2003, Vp/Vs from multicomponent seismic data and automatic PS to PP time mapping: SEG Technical Program Expanded Abstracts, **22**, 789–792.

Rickett, J., and P. Sava, 2001, Offset and angle domain common-image gathers for shot-profile migration: 71st Ann. Internat. Mtg, Soc. of Expl. Geophys., 1115–1118.

Sava, P., and I. Vasconcelos, 2010, Extended imaging condition for wave-equation migration: Geophysical Prospecting, in press.

Sava, P. C., and S. Fomel, 2003, Angle-domain common-image gathers by wavefield continuation methods: Geophysics, **68**, 1065–1074.

Shen, P., 2004, Wave-equation migration velocity analysis by differential semblance optimization: PhD thesis, Rice Univeristy.

Shen, P., C. Stolk, and W. Symes, 2003, Automatic velocity analysis by differential semblance optimization: 73th Annual International Meeting, SEG, Expanded Abstracts, 2132–2135.

Shen, P., and W. W. Symes, 2008, Automatic velocity analysis via shot profile migration: Geophysics, **73**, VE49–VE59.

Stewart, R. R., J. Gaiser, R. J. Brown, and D. C. Lawton, 2002, Converted-wave seismic exploration: Methods: Geophysics, **67**, 1348–1363.

———, 2003, Converted-wave seismic exploration: Applications: Geophysics, **68**, 40–57.

Yan, J., and P. Sava, 2008, Isotropic angle-domain elastic reverse-time migration: Geophysics, **73**, S229–S239.

Yang, T., and P. Sava, 2008, Wave-equation extended images for semblance and depth focusing velocity analysis: SEG Technical Program Expanded Abstracts, **27**, 2351–2355.

Yuan, J. J., G. Nathan, A. Calvert, and R. Bloor, 2008, Automated C-wave registration by simulated annealing: SEG Technical Program Expanded Abstracts, **27**, 1043–1047.